Influence of Low Amounts of Nanostructured Silica and Calcium Carbonate Fillers on the Large-Area Dielectric Breakdown Performance of Bi-axially Oriented Polypropylene

I. Rytöluoto[1], K. Lahti[1], M. Karttunen[2], M. Koponen[2], S. Virtanen[3], M. Pettersson[3]

[1]Tampere University of Technology, Department of Electrical Engineering, Tampere, Finland

[2]Technical Research Centre of Finland, Tampere, Finland

[3]Nanoscience Center, Department of Chemistry, University of Jyväskylä, Jyväskylä, Finland

***Abstract* — Influence of low amounts (1.0-2.0wt-%) of nanostructured silica and calcium carbonate fillers on the large-area dielectric breakdown performance of bi-axially oriented polypropylene (BOPP) is analyzed. A multi-breakdown measurement method based on the self-healing breakdown capability of metallized film is utilized for the breakdown characterization in order to cover relatively large total film areas, thus leading to results of higher relevance from the practical point-of-view. The dispersion and distribution qualities of filler particles at the nanoscale are evaluated with transmission electron microscopy (TEM) imaging. Weibull statistical analysis suggests that the breakdown distribution homogeneity can be improved with both the filler types. The 1.0wt-% silica-BOPP composite also shows a shift of the weakest points towards higher dielectric strength in comparison to the neat BOPP. However, with increasing filler content, new failure modes are introduced into the nanocomposites, hence decreasing the overall breakdown performance in the >5% breakdown probability region in comparison to the un-filled reference BOPP film.**

Keywords—Polymer nanocomposite film, polypropylene, silica, calcium carbonate, dielectric breakdown performance

I. Introduction

In recent years, an increasing amount of research on dielectric polymer nanocomposite films for next-generation capacitor applications has emerged and improvements in properties such as dielectric breakdown strength are aspired [1]. In general, potential improvements in the short-term breakdown performance may be achieved with polymer nanocomposites of permittivity-matching constituents and preferably with low nanoparticle fill-fractions, as demonstrated e.g. with nano-silica filled cross-linked polyethylene (XLPE) [2], core functionalized nano-silica filled epoxy [3] and nano-silica filled bi-axially oriented polypropylene (BOPP) films [4], [5], [6]. However, filler dispersion and distribution in the polymer matrix as well as the film processing conditions [6], [7] strongly affect the dielectric properties of the end-product and the potential advantageous effect of a smooth nanodispersion on the breakdown performance can be overwhelmed if micro-aggregates are present in the material, as reported e.g. in the case of nano-calcium-carbonate-filled BOPP films in [8]. Apart from the material composition and processing alone, accurate statistical knowledge of the breakdown performance is of fundamental importance during the development and optimization phase of novel dielectric films [9]. However, the current state-of-the-art dielectric breakdown measurement methods often result only in a limited amount of data, leading to poor statistical relevance and impaired evaluation of the breakdown performance [10]. In this paper, the influence of low amounts of nanostructured silica and calcium carbonate filler particles on the large-area dielectric breakdown performance of BOPP is studied. A multi-breakdown measurement method based on the self-healing breakdown capability of metallized film is utilized for the breakdown characterization in order to cover relatively large total sample areas with a slow rate-of-rise approach, thus leading to results of higher relevance from the practical point-of-view [10], [11]. The dispersion and distribution qualities of the filler particles at the nanoscale are evaluated with transmission electron microscopy (TEM) imaging.

II. Experimental

A. Film processing and sample details

The sample details along with the measured average film thicknesses and standard deviations are presented in Table 1. Unstabilized polypropylene homopolymer HC318BF in powder form (a non-commercial product from Borealis N.V.) was used as the matrix polymer. The filler loadings of 1.0wt-% and 2.0wt-% of Aerosil R812 S (hydrophobic fumed silica by Evonik) and Socal 322 (precipitated calcium carbonate (PCC) by Solvay) were studied. One of the compounds included both 1.0wt-% of silica and 1.0wt-% of PCC. Process stabilizer

TABLE I. Sample film details.

Sample code	Filler loading (wt-%)			*N* samples / total film area (cm²)	Film thickness (µm)	
	Planned		*Realized*		*Avg.*	*SD*
	Silica	PCC				
PP-Sil-1	1.0	-	1.14	10 / 810cm²	18.85	2.36
PP-Sil-2	2.0	-	2.24	10 / 810cm²	18.06	2.22
PP-PCC-1	-	1.0	0.80	10 / 810cm²	23.19	2.44
PP-PCC-2	-	2.0	1.87	10 / 810cm²	22.94	2.66
PP-Sil+PCC	1.0	1.0	1.62	10 / 810cm²	25.22	2.32
PP-Ref	-	-	-	6 / 486cm²	21.33	2.58

Irganox 1010 (0.47wt-%) and co-stabilizer Irgafos 168 (0.35wt-%) were added to the compounds. The processing was conducted at the VTT Technical Research Centre of Finland.

The raw powder materials were first pre-mixed manually in a polyethylene bag (approximate mixing time of 2 min) and thereafter compounded by a Berstorff ZE 25/48D twin screw compounder with high-shear screw geometry, two separate kneading sections and a melt filter (screen size 42μm). The compound was cooled in a water bath under a laminar air flow hood over the cooling section. Polymers were dried at 70°C for 1.5 hours in an oven and for 0.5 hour in a vacuum oven before the compounding. Cast films were then extruded by a Brabender Plasticorder single screw extruder with a three-layer screen pack. The single screw had three stages with a mixing zone and the compression was 4:1. The films (500-700μm) were cast through a 120mm slot die onto a chill roll at +90°C. Screw speed was 100rpm and cylinder temperatures were between 220°C and 230°C. Compounds were also dried before the cast film extrusion. Finally, the cast films were bi-axially oriented with a Brückner KARO IV film stretching machine (set temperature 157°C, stretching ratio 5.4x5.4). The realized filler amounts were determined by burning the organic polymer and additives in an oven at 600°C for 30min+10min (see Table 1) according to the ISO 3451-1 standard.

For the multi-breakdown measurement, sample films were cut to 110mm x 110mm dimensions from the bi-axially oriented film sheets. Sample film thicknesses were measured systematically at 25 points covering a 100mm x 100mm area with an LE1000-1 high-precision thickness measurement gauge (accuracy 0.1μm, resolution 0.05μm). The average film thicknesses with the standard deviations are presented in Table 1. Thickness deviation of the sample films was taken into account during the breakdown field calculation. In order to realize the self-healing breakdown capability, Zn-Al-metallized BOPP film (12μm Tervakoski PSX) was used as the electrode film. The sample film was sandwiched between two electrode films (metallized surfaces facing towards the sample film), thus forming a test capacitor with an active area of 81cm^2.

B. *Large-area multi-breakdown measurement*

The large-area breakdown measurement was based on the self-healing breakdown capability of metallized film which enables the measurement of multiple breakdowns from the sample area [6], [10], [11]. During the self-healing process, the fault spot is spontaneously isolated from the rest of the electrode due to the vaporization of small amount of metallization layer around the breakdown channel. The measurements were conducted in oil (Shell Diala DX) in accordance with IEC-60243 standard in order to mitigate surface flashovers. The DC voltage across the test capacitor was first raised to approximately 40-60% of the probable short-time breakdown voltage with a fast ramp speed of 400V/s, after which a slow ramp speed of 30V/s was used for measuring the self-healing breakdown events, roughly in accordance to the slow rate-of-rise test defined in the IEC-60243-1. The test setup and the procedure are discussed in more detail in [10].

During each discharge event in the test capacitor, the discharge current, test capacitor voltage and the time-signature of the event were recorded with a high-resolution oscilloscope operated in the sequence-acquisition mode and triggered to the positive rising edge of the discharge current signal. This allowed a detailed determination of the breakdown voltage, voltage drop, peak current, discharge energy and various pulse time parameters for each event. A video was recorded from the top of the test capacitor unit for the whole duration of the breakdown measurement, allowing detailed chronological analysis of the breakdown progression of the sample after the measurement. Breakdown fields were determined manually by rigorously determining the average thickness around the discharge spot (by means of the video recording) and by calculating the average breakdown field event-by-event in MATLAB.

C. *Breakdown data selection procedure*

A data selection procedure based on the discharge energy characteristics of the self-healing breakdown process was utilized for excluding non-breakdown events from the measurement data. It has been hypothesized that discharge events with the discharge energies and breakdown voltages not following the trend set by the first breakdowns may be attributed to successive breakdowns occurring close to or at previous breakdown sites or to other non-breakdown events (partial discharges, surface flashovers). The data selection was based on two criteria, namely by selecting only the discharge events (i) for which the corresponding discharge energies followed the trend preset by the first measured self-healing breakdowns and (ii) for which the breakdown voltages were higher than that of the previously selected breakdown. First breakdowns were used as a basis for the data selection procedure. The procedure is discussed in detail elsewhere [6], [10], [11].

D. *Statistical analysis*

For the statistical analysis of the breakdown data, 2-parameter Weibull distributions and additively mixed Weibull distributions were utilized:

$$F(x) = \sum_{i=1}^{S} \frac{N_i}{N} F_i(x) = \sum_{i=1}^{S} \frac{N_i}{N} \left[1 - \exp\left\{ -\left(\frac{x}{\alpha_i} \right)^{\beta_i} \right\} \right]. \qquad (1)$$

In (1), $F_i(x)$ is the 2-parameter Weibull distribution, S is the number of subpopulations, N_i/N is the portion (%) of the subpopulation i and α_i and β_i are the Weibull parameters of subpopulation i. The scale parameter α corresponds to the value of x at the 63.2% failure probability and the shape parameter β depicts the slope or homogeneity of the theoretical distribution. For a single 2-parameter Weibull distribution, S and the portion N_i/N in (1) are equal to 1 and 100%, respectively. Maximum-likelihood estimation (MLE) and non-linear regression (NLR) methods were used for the parameter estimation and the analysis was performed with Weibull++ and MATLAB software. 90% confidence bounds were calculated based on the Fisher Matrix (FM) method.

III. RESULTS AND DISCUSSION

A. *Structural characterization*

Figure 1 presents TEM-micrographs of ultrathin sections of the studied PP-composites. The ultrathin sections of the cast film samples were obtained using a Diatome 35° diamond knife at room temperature with a Leica Reichert Ultracut ultramicrotome. The 90nm thick sections were collected on a 400 mesh copper grid and imaged with a JEOL JEM-1400EX electron microscope. The dispersion state of the nanoparticles in all the composites was found to be similar and of heterogeneous nature. At the nanoscale, the filler material was partially well-dispersed in nanosized clusters but >100nm agglomerates were also observed. The TEM-images also revealed that PP-PCC-1 and PP-PCC-2 compounds contained silica, presumably due to a cross-contamination from the previously compounded silica-composites. Upon closer investigation of the 1.0wt-% silica-composite, micron-sized agglomerates were observed, and even though they were relatively scarce, they contained substantially high amounts of filler material. Thus, considering the densities of the nanoscale particle dispersions presented in Figure 1, all the compounds may contain micro-agglomerates.

B. Large-area breakdown performance

Large-area multi-breakdown distributions of the studied composites are presented in Figure 2 along with the 90% confidence bounds (shaded areas). If applicable, single 2-parameter Weibull distributions were fitted to the breakdown data; otherwise mixed Weibull distributions (2-3 subpopulations) were utilized on the basis of the best goodness-of-fit test result. In order to enable convenient comparison between all the distributions regardless of the distribution structure, 5%, 63.2% and 95% breakdown percentiles and the weakest points measured from the total film areas are presented in Table 2.

Figure 2 and Table 2 together indicate that in comparison to the unfilled BOPP film, the inclusion of 1.0 and 2.0wt-% of either silica or PCC filler decreases the breakdown performance in the >5% breakdown probability region but also leads to a concurrent improvement of the breakdown distribution homogeneity. In the case of silica filler, the difference between 1.0wt-% and 2.0wt-% fill-fractions is distinguishable (Figure 2a) whereas the compounds with 1.0wt-% and 2.0wt-% of PCC together show a very similar breakdown performance (Figure 2b). The compound PP-Sil+PCC with both silica and PCC fillers shows the highest breakdown distribution homogeneity with the Weibull β of 22.14 in comparison to the 11.65 of the reference BOPP, however, its breakdown performance in the >5% breakdown probability region is the lowest of all the studied compounds. The 1.0wt-% silica composite (PP-Sil-1) stands out from the rest of the composites as it shows both the improvement of breakdown distribution homogeneity and the shift of weak points towards higher dielectric strength in comparison to the

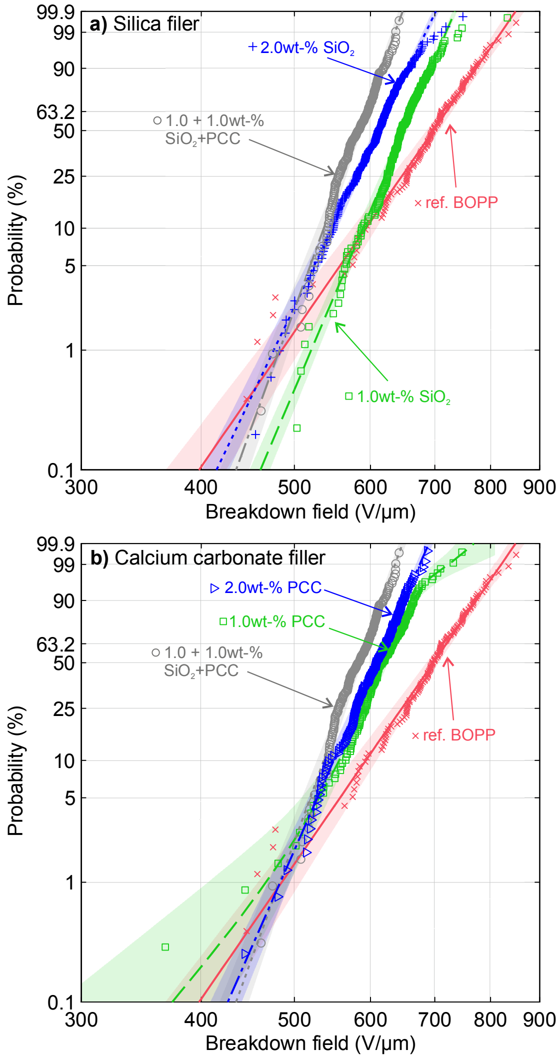

Fig. 2. Effect of **a)** silica and **b)** calcium carbonate fillers on the large-area multi-breakdown performance of BOPP. The shaded areas represent the 90% confidence bounds.

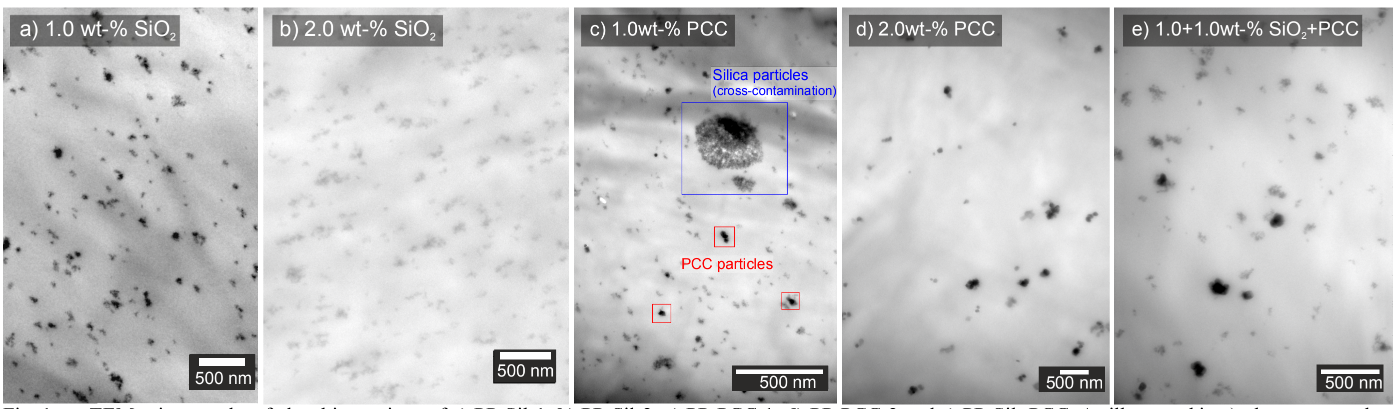

Fig. 1. TEM-micrographs of ultrathin sections of **a)** PP-Sil-1, **b)** PP-Sil-2, **c)** PP-PCC-1, **d)** PP-PCC-2 and **e)** PP-Sil+PCC. As illustrated in c), the compounds PP-PCC-1 and PP-PCC-2 showed small amounts of silica particles, presumably due to a cross-contamination from the previously compounded silica-materials.

neat BOPP film, see Figure 2a. It should be noted that from the practical point-of-view, both the increase of breakdown distribution homogeneity (Weibull β) and the improvement in the low-probability breakdown behavior are substantially more relevant than the breakdown behavior in the higher (>10%) breakdown probability region.

C. Discussion

The trends observable in the large-area breakdown responses are not merely attributable to the filler contents (see Table 1 for the realized filler contents) but rather they reflect the filler-matrix interaction, nanodispersion and the degree of micro-aggregation over large film volumes. The decrease in the breakdown performance with increasing filler content is consistent with previous reports on various amorphous polymer-silica nanocomposites [12], polystyrene-silica nanocomposites [13] and BOPP-PCC nanocomposites [8]. The composites studied here also exhibited improvements in the breakdown distribution homogeneity. In coherence with [12], the nano fillers seem to introduce a lower energy failure mode into the polypropylene matrix, but due to the relatively uniform dispersion at the nanoscale, the breakdown variability is concurrently reduced in comparison to the neat polypropylene.

The role of the antioxidants in the final breakdown performance should also be considered. Although not studied here, the co-stabilizer Irgafos 168 has been shown to have a detrimental effect on the breakdown distribution homogeneity of BOPP films [6] and likewise, residues of the main process stabilizer Irganox 1010 may also impair the breakdown strength of BOPP [14]. Further, the interaction between the antioxidants and the nanofillers should also be considered, as a substantial amount of antioxidant may be adsorbed on the filler surfaces as discussed e.g. in the case of poly(ethylene-*co*-butyl acrylate)-Al_2O_3 nanocomposites and Irganox 1010 in [15]. Initial antioxidant adsorption on the nanofiller surfaces, film processing and the possible slow-release of the antioxidant residue from the adsorption sites over time may have an influence on both the short- and long-term breakdown performance of the end-product, and should be investigated further in the future.

IV. CONCLUSIONS

Inclusion of low fill-fractions of silica and/or calcium carbonate nanoparticles in BOPP was found to decrease the large-area multi-breakdown performance in the >5% breakdown probability region but also lead to concurrent improvements in the breakdown distribution homogeneity in comparison to the unfilled reference. The 1.0wt-% silica composite (PP-Sil-1) stood out from the rest of the composites as it showed both the improvement of the breakdown distribution homogeneity and a shift of weak points towards higher dielectric strength. The results point that the optimum nanofiller content resides at the low fill fraction level where it is more probable to achieve good-quality nanodispersion without excess micro-agglomeration over large volumes. The study also exemplified the utilization of large-area multi-breakdown approach for measuring breakdown performance of relatively large film areas with high statistical accuracy.

TABLE II. LARGE-AREA BREAKDOWN PERCENTILES.

Sample code	*n*	Breakdown field (V/µm)			Weakest point (V/µm)
		5%	*63.2%*	*95%*	
PP-Sil-1	224	567 (560…575)	664 (659…668)	703 (699…707)	503
PP-Sil-2	253	524 (515…533)	626 (621…630)	668 (664…671)	456
PP-PCC-1	174	531 (515…547)	634 (629…639)	679 (669…689)	367
PP-PCC-2	198	528 (519…538)	621 (617…625)	660 (655…664)	444
PP-Sil+PCC	161	519 (511…528)	594 (590…598)	624 (620…628)	462
PP-Ref	128	558 (539…578)	720 (711…729)	791 (780…802)	446

[a] *n* indicates the number of qualified breakdowns after the data selection procedure.
[b] Numbers in parenthesis denote the 90% confidence bounds.

REFERENCES

[1] J. Keith Nelson, Dielectric Polymer Nanocomposites.: Springer US, 2010.

[2] M. Roy, J. K. Nelson, R. K. MacCrone, and L.S. Schadler, "Candidate mechanisms controlling the electrical characteristics of silica/XLPE nanodielectrics," *Journal of Materials Science*, vol. 42, no. 11, pp. 3789-3799, 2007.

[3] S. Virtanen et al., "Dielectric breakdown strength of epoxy bimodal-polymer-brush-grafted core functionalized silica nanocomposites," *IEEE Transactions on Dielectrics and Electrical Insulation*, vol. 21, no. 2, pp. 563-570, 2014.

[4] M. Takala et al., "Dielectric properties and partial discharge endurance of polypropylene-silica nanocomposite," *IEEE Transactions on Dielectrics and Electrical Insulation*, vol. 17, no. 4, pp. 1259-1267, 2010.

[5] M. Takala et al., "Effect of low amount of nanosilica on dielectric properties of polypropylene," in *10th IEEE International Conference on Solid Dielectrics (ICSD)*, 2010, pp. 1-5.

[6] I. Rytöluoto et al., "Large-Area Dielectric Breakdown Performance of Polymer Films – Part II: Interdependence of Filler Content, Processing and Breakdown Performance in Polypropylene-Silica Nanocomposites," *IEEE Transactions on Dielectrics and Electrical Insulation*, (under review), 2014.

[7] C. Calebrese, Le Hui, L.S. Schadler, and J.K. Nelson, "A review on the importance of nanocomposite processing to enhance electrical insulation," *IEEE Transactions on Dielectrics and Electrical Insulation*, vol. 18, no. 4, pp. 938-945, 2011.

[8] Virtanen S. et al., "Structure and dielectric breakdown strength of nano calcium carbonate/polypropylene composites," *Journal of Applied Polymer Science*, vol. 131, no. 1, 2014.

[9] M.A. Schneider, J.R. MacDonald, M.C. Schalnat, and J.B. Ennis, "Electrical breakdown in capacitor dielectric films: Scaling laws and the role of self-healing," in IEEE International Power Modulator and High Voltage Conference (IPMHVC), 2012, pp. 284-287.

[10] I. Rytöluoto, K. Lahti, M. Karttunen, and M. Koponen, "Large-Area Dielectric Breakdown Performance of Polymer Films – Part I: Measurement Method Evaluation and Statistical Considerations on Area-Dependence," *IEEE Transactions on Dielectrics and Electrical Insulation*, (under review), 2014.

[11] I. Rytöluoto and K. Lahti, "New Approach to Evaluate Area-Dependent Breakdown Characteristics of Dielectric Polymer Films," *IEEE Transactions on Dielectrics and Electrical Insulation*, vol. 20, no. 3, pp. 937-946, 2013.

[12] A. Grabowski Christopher et al., "Dielectric Breakdown in Silica–Amorphous Polymer Nanocomposite Films: The Role of the Polymer Matrix," *ACS Applied Materials & Interfaces*, vol. 5, no. 12, pp. 5486-5492, 2013.

[13] M. Praeger, A.S. Vaughan, and S.G. Swingler, "The breakdown strength and localised structure of polystyrene as a function of nanosilica fill-fraction," in *IEEE International Conference on Solid Dielectrics (ICSD)*, 2013, pp. 863-866.

[14] J. Ho, R. Ramprasad, and S. Boggs, "Effect of Alteration of Antioxidant by UV Treatment on the Dielectric Strength of BOPP Capacitor Film," *IEEE Transactions on Dielectrics and Electrical Insulation*, vol. 14, no. 5, pp. 1295-1301, 2007.

[15] S. Nawaz, P. Nordell, H. Hillborg, and U.W. Gedde, "Antioxidant activity in aluminium oxide – poly(ethylene-co-butyl acrylate) nanocomposites," *Polymer Degradation and Stability*, vol. 97, no. 6, pp. 1017-1025, 2012.